Electronic Structure, Heisenberg Coupling Constants, and Metal−Metal Bond in Dimeric Iron(II) Organometallics with the Metal Centers at Variable Distances: A Density Functional Approach

Paola Belanzoni, Nazzareno Re, Marzio Rosi, and Antonio Sgamellotti*

Dipartimento di Chimica, Università di Perugia, via Elce di Sotto 8, 06123 Perugia, Italy

Evert Jan Baerends

Scheikunding Laboratorium, Vrije Universiteit, De Boelelaan 1083,
1081 HV Amsterdam, The Netherlands

Carlo Floriani

Institut de Chimie Minérale et Analytique, BCH, Université de Lausanne,
CH-1015 Lausanne, Switzerland

Received June 23, 1995[⊗]

Density functional calculations were performed to investigate the electronic structure, the magnetic coupling, and the bonding in $Fe_2(NCH_2)_2(NCH)_2(C_6H_5)_2$, $Fe_2(C_6H_5)_4$, and $Fe_2(HNCH)_4$ model systems. The corresponding real compounds are characterized by strongly reduced magnetic moments, while metal−metal distances vary in a wide range from uncommonly short to slightly long. The results show the absence of a direct Fe(II)−Fe(II) bond for the first two compounds: both the electronic structure studies and the Heisenberg coupling analysis give indications in this direction. The reduced magnetic moment results essentially from strong antiferromagnetic interactions via bridging ligands. Heisenberg coupling constants were calculated for each complex, which show an antiferromagnetic coupling of four unpaired electrons on each center. In the third compound there is a relevant direct Fe−Fe interaction, although the short Fe−Fe distance results mainly from a strong metal-bridging ligand interaction.

1. Introduction

There has recently been considerable interest in the synthetic and structural chemistry of dinuclear Fe(II) metal complexes showing short metal−metal distances.[1,2] In particular some of these complexes show interesting magnetic properties which have been employed in a recent paper as a diagnostic for the presence of iron−iron bond.[2] This is a very unusual behavior for organometallic complexes, since metal−metal bonds are nearly always associated with diamagnetism. Actually the observed magnetic behaviors, especially for complexes with the shortest Fe−Fe distances, may show complicated patterns with a decrease in magnetic moments from the values for isolated Fe(II) species and cannot always be interpreted in terms of Heisenberg exchange between two weakly interacting metal centers. For one complex, a fairly isolated spin state with relevant zero-field splitting has been found—in analogy with what has been observed for some ruthenium binuclear complexes[3]—and the magnetic behavior is difficult to interpret in a definitive and unambiguous way. The situation is therefore far from being completely clear, and a theoretical investigation would be very useful in elucidating the electronic structure of these complexes and the presence of a direct metal−metal bond.

This paper is addressed to the theoretical study of a series of dinuclear iron(II) compounds recently synthesized and structurally and magnetically characterized by Floriani and co-workers.[2] Three well-characterized compounds have been considered: $[(PhCN)_2(Mes)_2Fe_2\{\mu\text{-}N{=}C(Mes)(Ph)\}_2]$ (**1**), $[Fe_2Mes_4]$ (**2**), and $[\{\eta^2\text{-}C(Mes){=}NBu^t\}_2Fe_2\{\mu\text{-}C(Mes){=}NBu^t\}_2]$ (**3**) (Mes = 2,4,6-$Me_3C_6H_2$), which show Fe−Fe distances of 2.859, 2.614, and 2.371 Å, respectively (see Figure 1). Magnetic susceptibility data, in the temperature range 1.9−310 K, were collected and interpreted by Floriani and co-workers:[2] the data for complex **1** have been interpreted with a Heisenberg spin Hamiltonian by considering the coupling of two $S_1 = S_2 = 2$ Fe(II) centers; on the other hand, the data for complex **2** could not be interpreted with a Heisenberg spin Hamiltonian, requiring the use of a non-Heisenberg spin ladder, although an average coupling constant could be defined for the spin states up to $S = 3$.

Moreover, for complex **2**, the $S = 4$ state was found to be negligibly populated, even at room temperature, and therefore at least 1000 cm^{-1} higher in energy than the ground state: this implies that two of the unpaired electrons belonging to the iron atoms are essentially paired off, although it cannot be deduced if this is due to a strong antiferromagnetic coupling through the mesityl bridge or to a direct Fe−Fe interaction. The fairly short Fe−Fe distance (2.614 Å to be compared to 2.48 Å in metallic iron) which lies in the range expected for a single bond[4] would suggest a direct iron−iron interaction, but no definitive

---

[⊗] Abstract published in *Advance ACS Abstracts,* November 15, 1996.

(1) Cotton, F. A.; Daniels, L. M.; Falvello, L. R.; Murillo, C. A. *Inorg. Chim. Acta* **1994**, *219*, 7.

(2) Klose, A.; Solari, E.; Floriani, C.; Chiesi-Villa, A.; Rizzoli, C.; Re, N. *J. Am. Chem. Soc.* **1994**, *116*, 9123.

(3) Cotton, F. A.; Walton, R. A. *Multiple Bonds between Metal Atoms*; Clarendon: Oxford, U.K., 1993.

(4) Fehlhammer, W. P.; Stolzenberg, H. Dinuclear Iron Compounds with Hydrocarbon Ligands. In *Comprehensive Organometallic Chemistry*; Wilkinson, G., Stone, F. G. A., Abel, E. W., Eds.; Pergamon: Oxford, U.K., 1982; Vol. 4, Chapter 31.4.

S0020-1669(95)00767-1 CCC: $12.00

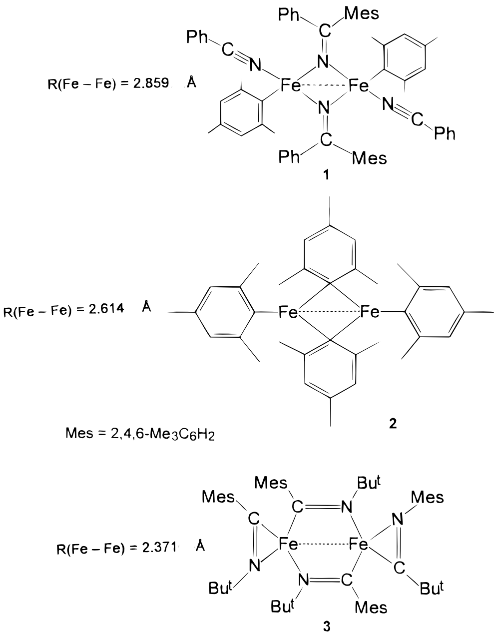

Figure 1. Synthesized complexes.

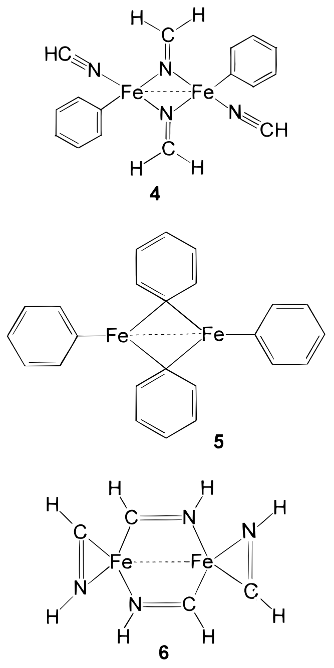

Figure 2. Model systems studied.

conclusion on the existence of a localized σ Fe−Fe bond can be obtained from the experimental data. A theoretical investigation is therefore necessary to elucidate the presence of a direct Fe−Fe bond. The magnetic data for compound **3** show the typical behavior for two spin centers with a small antiferromagnetic Heisenberg coupling: the magnetic moment per iron as a function of the temperature is essentially constant from room temperature down to about 40 K and then slowly decreases. However, the $\mu_{\mathrm{eff}} = 3.86\ \mu_{\mathrm{B}}$ value of the magnetic moment in the 40−310 K range corresponds exactly to three unpaired electrons, and as a matter of fact the magnetic data were well-fitted with a Heisenberg spin Hamiltonian for the coupling of two $S_1 = S_2 = {}^3/_2$ spin centers, giving a reasonable g factor of $g = 1.98$ and a small coupling constant $J = -0.45$ cm^{-1}. This has been interpreted as being due to the strong coupling of one of the four unpaired electrons per iron atom and would support a Fe−Fe single bond. Moreover, the small value obtained for the coupling constant, $J = -0.45$ cm^{-1}, implies a very small antiferromagnetic interaction between the remaining three unpaired electrons for iron and would suggest the absence of any π or δ bonding, in spite of the short Fe−Fe distance which is close to that expected for a Fe−Fe double bond.[4] However, we recall that the assignment of metal−metal bond order on the basis of metal−metal distances tends to be ambiguous when bridging ligands are present.[3] A theoretical study, therefore, would also be useful for this compound for elucidating the nature of the Fe−Fe bond.

In this paper we have performed LCAO−local density functional (LDA) valence bond calculations on $Fe_2(NCH_2)_2(NCH)_2(C_6H_5)_2$ (**4**), $Fe_2(C_6H_5)_4$ (**5**), and $Fe_2(HNCH)_4$ (**6**) molecules (see Figure 2), taken as models of compounds **1**−**3**, in order to examine the nature of the metal−metal and metal−ligand bonding in these complexes. While for compounds **4** and **5** we have found that the reduced magnetic moment results essentially from a strong electron coupling through superexchange via bridging ligands and the energy levels follow a Heisenberg spin ladder, for compound **6** we have found a non-Heisenberg spin ladder, with an isolated quintet ground state showing a relevant metal−metal interaction.

This theoretical result for model complex **6** has suggested interpretation of the magnetic data observed for compound **3** by using a phenomenological model, different from that used in ref 2, in which the whole dimer is considered an isolated spin center with $S = 2$. We have therefore performed a new fitting of μ_{eff} vs T data for complex **3**, using an axial spin Hamiltonian, obtaining an agreement as good as the original fitting performed in ref 2. In order to distinguish between these two interpretations, we studied the magnetization of compound **3** at high fields, taking isothermal variable-field magnetization measurements at 1.9 K, up to 5.5 T. The result of this study seems to confirm that the model of the dimer as one spin center with $S = 2$ proposed in this paper is more appropriate.

Such an approach, in which theoretical and phenomenological techniques are combined together, is particularly suitable for studying dinuclear paramagnetic complexes with direct metal−metal interactions, like compound **3**, where magnetic data alone are not sufficient for giving definite conclusions on the nature of the metal−metal bonding. It gives a better understanding of the correlations between structure and magnetic properties and more insight into the electronic structure of these systems.

Experimental Section. Magnetic susceptibility measurements were made with a Quantum Design Model MPMS5 SQUID magnetometer operating at a magnetic field strength of 3 kOe, in the temperature range 1.9−310 K. Corrections were applied for diamagnetism, calculated from Pascal constants. Effective magnetic moments were calculated by the equation $\mu_{\mathrm{eff}} = 2.828(\chi_{\mathrm{Fe}}T)^{1/2}$ where χ_{Fe} is the magnetic susceptibility per iron. Fitting of the magnetic data to the theoretical expression was performed by minimizing the agreement factor, defined as

$$R = \sum \frac{[\chi_i^{\mathrm{obsd}}T - \chi_i^{\mathrm{calcd}}T]^2}{(\chi_i^{\mathrm{obsd}}T)^2}$$

through a Levenberg−Marquardt routine.[5] Variable-field magnetization data were measured on the same susceptometer at 1.9 and 6.0 K, in the range 3−55 kG, and fitted to the theoretical expressions through the same routine.

2. Computational and Methodological Details

All calculations were performed on $Fe_2(NCH_2)_2(NCH)_2(C_6H_5)_2$ (**4**), $Fe_2(C_6H_5)_4$ (**5**), and $Fe_2(HNCH)_4$ (**6**) systems by using the Amsterdam

---

(5) Press, W. H.; Flannery, B. P.; Teukolsky, S. A.; Vetterling, W. T. *Numerical Recipes*; Cambridge University Press: Cambridge, U.K., 1989.

density functional (ADF) program elsewhere described,[6] which has been applied extensively in the field of transition metal chemistry,[7] especially in the analysis of the nature of metal−metal bonding in dinuclear complexes.[8] The LDA density functional approach was used together with the Vosko−Wilk−Nusair parametrization for the exchange-correlation potential and the Becke[9] and Perdew[10] nonlocal corrections to the energy. The basis set consisted of Slater type atomic orbitals (STOs). The frozen core approximation allowed for the evaluation of the valence orbitals which are orthogonalized onto the core by augmenting the valence set with a single-ζ STO for each core type orbital. Core orbitals were frozen for C(1s), N(1s), and Fe(1s,2s,2p). The valence basis set we used can be briefly described as follows: H(double ζ, 1s); C and N (double ζ, 2s; double ζ, 2p); Fe(double ζ, 3s; double ζ, 3p; triple ζ, 3d; triple ζ, 4s; single ζ, 4p). Geometrical parameters were taken from experimental structural X-ray data[2] for all of the molecules. The geometry of $Fe_2(C_6H_5)_4$ was deduced from that of $[Fe_2Mes_4]$, replacing the mesityl ligands with phenyls; that of $Fe_2(NCH_2)_2(NCH)_2(C_6H_5)_2$ was deduced from the geometry of $[(PhCN)_2(Mes)_2Fe_2\{\mu\text{-}N{=}C(Mes)(Ph)\}_2]$, replacing the mesityl ligands bonded to Fe with phenyls and the phenyls and the mesityls bonded to C with hydrogen atoms; and that of $Fe_2(HNCH)_4$ was deduced from the geometry of $[\{\eta^2\text{-}C(Mes){=}NBu^t\}_2Fe_2\{\mu\text{-}C(Mes){=}NBu^t\}_2]$, replacing the mesityl ligands bonded to C and the tertiary butyls bonded to N with hydrogen atoms. The Fe—Fe distance decreases from 2.859 Å for complex **4** to 2.614 Å for **5** to 2.371 Å for **6**. For molecule **4**, the remaining geometrical parameters were as follows: Fe—N* = 2.018 Å (the star designates bridging atoms or groups from now on), Fe—N = 2.091 Å, Fe—C = 2.118 Å, N*—C* = 1.262 Å, C*—H* = 0.95 Å, N—C = 1.137 Å, C—H = 0.95 Å, with H*C*H* angle of 120°. The iron atom is roughly tetrahedrally coordinated to two bridging groups and to two terminal ligands, so that the model is consistent with the C_{2h} point group. The phenyl rings lie perpendicularly to the Fe_2N_2 plane. For molecule **5**, we assumed idealized C_6H_5 rings with a C—C distance of 1.40 Å and a C—H distance of 0.95 Å; the Fe—C* distance was 2.165 Å, while the Fe—C was 2.064 Å and the symmetry was idealized to D_{2h}. The two bridging phenyl rings lie perpendicularly to the Fe_2C_2 plane, while the two terminal phenyls lie parallel to it. Finally, for complex **6**, we assumed Fe—N* = 1.987 Å, Fe—N = 2.007 Å, N—C(=N*—C*) = 1.265 Å, Fe—C* = 1.968 Å, Fe—C = 1.921 Å, N—H(=N*—H*) = 0.90 Å, and C—H(=C*—H*) = 0.95 Å. The dimer contains terminal η^2-C,N and bridging μ_2-C,N iminoacyl moieties. The six-membered bimetallic ring has a boat conformation with dihedral angle between the two mean planes (individuated by Fe left, C, N, and Fe right) of 104.0°. A coordination plane is also defined by each of the Fe, C, N, C*, and N* groups of atoms, from which iron is displaced by 0.160 Å in the direction of the other iron. The total symmetry is C_2. For complexes **4** and **5** the coordinate system has been chosen so that the *z* axis is the main symmetry axis, while for complex **6** the *z* axis has been chosen as the Fe—Fe direction to simplify the bond analysis. In order to analyze the interaction between the atomic or molecular fragments constituting the systems, we used a decomposition scheme of the total bond energy presented elsewhere.[11] In our case Fe ($3d^84s^0$), C_6H_5, NCH, and NCH_2 were taken as fragments for complex **4**, Fe ($3d^84s^0$) and C_6H_5 for complex **5**, and Fe ($3d^84s^0$) and HNCH for complex **6**. To study the magnetic coupling, by determining the Heisenberg coupling constant between the two Fe centers, we adopted the broken symmetry spin unrestricted approach. This method has been applied to 2-Fe ferredoxin models by Noodleman and Baerends[12] and Noodleman and co-workers[13] and to 4-Fe ferredoxin models by Aizman and Case.[14] Through the relaxation of the total spin and spatial symmetry constraints, it is possible to achieve a description of the systems in which the Fe centers are both high spin and may be ferromagnetically or antiferromagnetically coupled. In the former case both sites show spin up, so that an overall high-spin situation arises; in the latter case one site shows spin up and the other site spin down, the overall system being in a low-spin state. To reach this goal, we removed the inversion center for complex **4**, lowering the symmetry from the C_{2h} geometrical symmetry to C_s and the mirror plane for complex **5** lowering the symmetry from D_{2h} to C_{2v}. When the orbitals are optimized in the spin-polarized self-consistent field (SCF) procedure, a broken symmetry SCF wave function is constructed in which the α-spin 3d electrons localize on one Fe and the corresponding β-spin 3d electrons localize on the opposite Fe, both subunits having high spin. This broken symmetry, spin-unrestricted wave function contains the physical interactions which enter, through the application of the second-order perturbation theory, in the Heisenberg coupling model,[15] described by a phenomenological Hamiltonian of the form $H = -2J\mathbf{S}_1\cdot\mathbf{S}_2$. Besides, the broken symmetry solution is not a spin eigenfunction, but it can be written as a superposition of pure spin states with $S = 0$ to $S = S_{\max} = S_1 + S_2$, whose weighting coefficients can be determined by using spin-projection techniques.[16] This allows one to relate the energy of the broken symmetry function (E_B) to that of the spin eigenstates in a very simple way. Expressing the spacing between the $S_{\max} + 1$ pure spin states (Heisenberg "spin ladder") in terms of the Heisenberg coupling constants J, $E(S) - E(S-1) = -2JS$, the knowledge of the energies of the broken symmetry function and of only one pure spin function is sufficient to determine J. In particular, if we consider the high-spin state ($S = S_{\max}$), which can be approximated as a single, spin-unrestricted determinant constructed with spin up on both sites of the molecule in full spatial symmetry, we can compute J from the relation[16]

$$E(S_{\max}) - E_B = -S^2_{\max}J \qquad (1)$$

The type of coupling determines the energy ordering (depending on the sign of *J*) and spacing (depending on the magnitude of *J*) of the various *S* states, and the magnetic properties of the systems will ultimately depend on the *S* value of the ground state and on how accessible the excited states are at room temperature.

Preliminary broken symmetry calculations performed on the $Fe_2(HNCH)_4$ molecule **6**, considered as a model for compound **3**, gave results qualitatively different from those obtained for molecules **4** and **5** and led to a non-Heisenberg spin ladder in contradiction with the interpretation of the magnetic behavior. The main difference between the results for compound **6** and those for compounds **4** and **5** is that when we build the broken symmetry wave function, we get three unpaired electrons with spin up mainly localized on the left and three with spin down on the right, but no choice of the occupations can be found which permits us to identify three couples of singly occupied orbitals with definite d and left or right character. All of the singly occupied orbitals are weakly polarized and have a strongly mixed metal bridging ligand character. Moreover, there are always at least two unpaired orbitals with strongly mixed left and right character. This suggested to us that some of the unpaired electrons on the metal fragments would strongly interact in the complex, making the broken symmetry approach questionable. To investigate this point, we therefore performed an independent unrestricted calculation on a pure spin state with spin number $S = 2$ lower than $S_{\max} = 3$, finding an energy much lower than the broken symmetry state and the $S = S_{\max}$ state, *i.e*, a non-Heisenberg spin ladder. Moreover, the analysis of the unrestricted wave function for the $S = 2$ ground state, discussed below, has clearly shown that there is a strong interaction between the two metal centers in complex **3**, and this makes no more valid some of the assumptions made in the development of the BSS approach. Therefore, for this complex we have dismissed the broken symmetry approach and considered all of the possible spin states from $S = 0$ to $S = 4$ in the full symmetry of the molecule (C_2), approximating them by unrestricted SCF calculations on the $M_S = 0-4$ wave functions.

---

(6) Baerends, E. J.; Ellis, D. E.; Ros, P. *Chem. Phys.* **1973**, *2*, 42. Baerends, E. J.; Ros, P. *Chem. Phys.* **1973**, *2*, 51; **1975**, *8*, 41.

(7) Baerends, E. J.; Rozendaal, A. In *Quantum Chemistry, The Challenge of Transition Metals, and Coordination Chemistry*.; Veillard, A., Ed.; D. Reidel Publ. Company: Dordrecht, The Netherlands, 1986; pp 159−177.

(8) Ziegler, T. *J. Am. Chem. Soc.* **1985**, *107*, 4453, and references cited therein.

(9) Becke, A. D. *Phys. Rev. A* **1988**, *38*, 3098.

(10) Perdew, J. P. *Phys. Rev. B* **1986**, *33*, 8822; **1986**, *34*, 7046.

(11) Ziegler, T.; Rauk, A. *Theor. Chim. Acta* **1977**, *46*, 1; *Inorg. Chem.* **1979**, *18*, 1558.

(12) Noodleman, L.; Baerends, E. J. *J. Am. Chem. Soc.* **1984**, *106*, 2316.

(13) Norman, J. C., Jr.; Ryan, P. B.; Noodleman, L. *J. Am. Chem. Soc.* **1980**, *102*, 4279.

(14) Aizman, A.; Case, D. A. *J. Am. Chem. Soc.* **1982**, *104*, 3269.

(15) Noodleman, L.; Case, D. A. In *Advances in Inorganic Chemistry*; Academic Press: New York, **1992**; Vol. 38, pp 423−470, and references cited therein.

(16) Noodleman, L. *J. Chem. Phys.* **1981**, *74*, 5737.

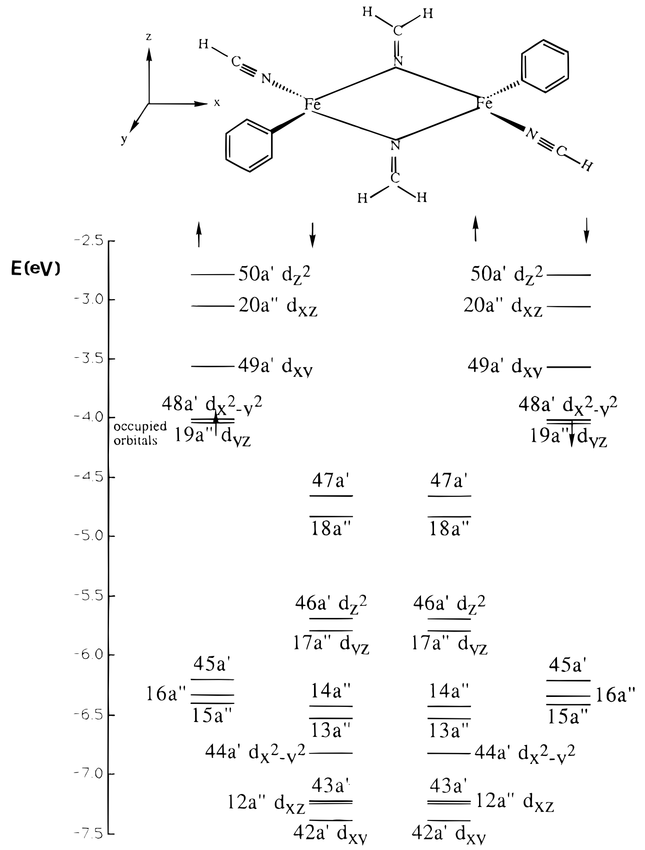

Figure 3. Energy levels for the broken symmetry state of $Fe_2(NCH_2)_2(NCH)_2(C_6H_5)_2$. The orbitals are grouped according to their distribution on the left or right of the molecule. Spin-up levels are shown below the up arrows; spin-down, below the down arrows. The six occupied and four unoccupied orbitals with mainly Fe 3d character are explicitly labeled.

However, a check of the expectation value for $\hat{S}^2$ has revealed a very small spin contamination of these unrestricted wave functions, confirming that they are good approximations of the pure spin states.

3. Results and Discussion

$Fe_2(NCH_2)_2(NCH)_2(C_6H_5)_2$ Complex. (a) Energy Level Structure. The energy level diagram (only the most important MO's) for the broken symmetry state (low spin, $M_S = 0$) of $Fe_2(NCH_2)_2(NCH)_2(C_6H_5)_2$ in C_s symmetry is shown in Figure 3. The picture is consistent with an antiparallel coupling of two high-spin subunits, each with spin vector $S = 2$. The diagram is organized in such a way that the orbitals are arranged in columns according to their spatial distribution on the left and right of the molecule and according to the spin index. The geometrical equivalence between the left and right halves of the homonuclear dimer explains the energetic degeneracy of each spin-up level on the left with its mirror-image spin-down orbital on the right. Besides, it is possible to recognize up-spin/down-spin pairs with large (or weak, in the case of the metal atoms) spatial overlap resembling still doubly occupied orbitals, as, for example, 14a″ ↑ (2a″ C_6H_5 right) and 15a″ ↓ (2a″ C_6H_5 right). These pairs can be degenerate or split, depending on how strong is the spin polarization. In the case of the "mainly" Fe 3d orbitals, this is particularly evident. On the right, the occupied spin-up Fe 3d orbitals, also called "magnetic" orbitals, are strongly stabilized by spin polarization and are metal−ligand bonding, while the corresponding spin-down Fe 3d orbitals are destabilized and lie in the virtual spectrum. The situation on the left is reversed, as the mirror image of that on the right. Therefore, from now on we will focus our attention on the right side.

(b) Population Analyses. In Table 1, we report the Mulliken population analysis of complex **4** for the important occupied and virtual orbitals in terms of Fe, NCH_2, NCH, and C_6H_5 fragments. Before commenting on the data, it is useful to give some description of the ligand (terminal and bridging) orbitals involved in these interactions. The 12a′ C_6H_5 orbital is the orbital containing, in C_s symmetry, the unpaired electron of the phenyl radical, being an sp^2 hybrid localized on the C not linked to H. The 2a″ and 3a″ orbitals represent the π occupied orbitals. The NCH ligand shows two available orbitals for bonding with the Fe atom: the occupied orbital 4a′, which turns out to be an sp hybrid, containing the nitrogen lone pair, and the two degenerate empty orbitals 5a′ and 2a″, which are of π^* type. The NCH_2 imino bridge ligand presents, in C_{2v} symmetry, two interesting orbitals: $2b_1$, which contains the unpaired electron and is localized mainly on a p orbital on the nitrogen atom, and $3a_1$, which is doubly occupied, containing the nitrogen lone pair, and is of sp hybrid nature. A calculation performed on the two bridging ligands, $(NCH_2)_2$, in C_{2h} symmetry, gave rise to two combinations of the $3a_1$ orbitals, $3a_u(3a_1 - 3a_1)$ and $3a_g$ $(3a_1 + 3a_1)$, and to two combinations of $2b_1$ orbitals, $3b_u$ $(2b_1 + 2b_1)$ and $3b_g$ $(2b_1 - 2b_1)$, which will result in being important in describing the composition of the complex MO's. In most of the higher occupied orbitals reported in Table 1 we can see a considerable Fe 3d character. The spin-up orbitals are strongly localized on the right side (Fe and terminal NCH, C_6H_5) of the molecule. The lowest unoccupied orbitals have from 50 to 76% Fe 3d character, with the remaining on the bridges and on the terminal ligands. Defining magnetic spin-up Fe 3d orbitals on the right is not completely without ambiguity, since all of the occupied orbitals are quite delocalized, but we could still attribute such a "label" with some confidence, looking closely at the MOs composition. Most of the orbitals reported in Table 1 are delocalized on the metals and the bridging or terminal ligands. The complete identification of the magnetic orbitals is quite difficult, but we determined them as 12a″, 17a″, 42a′, 44a′, and 46a′, corresponding mainly to $3d_{xz}$, $3d_{yz}$, $3d_{xy}$, $3d_{x^2-y^2}$, and $3d_{z^2}$, respectively. The $3d_{yz}$ Fe right orbital turns out to be doubly occupied. About this question, *i.e.*, the criterium we followed in choosing which of the five d orbitals should be doubly occupied, we must say that a calculation performed with the $3d_{x^2-y^2}$ orbital doubly occupied (which was the most reasonable alternative to $3d_{yz}$), gave a broken symmetry state with higher energy (−26.95 eV against the −27.20 eV we found before). Moreover, the previous analysis does not show any evidence of a possible direct iron−iron bond. The more relevant coupling mechanism turns out to be a strong antiferromagnetic coupling with bridging ligands assisting the electron exchange, but we will return to this point later.

$Fe_2(C_6H_5)_4$ Complex. (a) Energy Level Structure. In Figure 4, we present the energy level diagram for the broken symmetry state of the $Fe_2(C_6H_5)_4$ molecule in C_{2v} symmetry. The orbitals are grouped in columns according to their distribution on the left, middle, or right of the molecule and their spin. The interpretation of this diagram follows the same analysis we explained before, in the case of complex **4**. Again the system consists of two high-spin subunits, each with spin vector $S = 2$ coupled with antiparallel alignment of the spin vectors. Again we can observe the mirror image characteristic of each spin-up level with each corresponding spin-down level and the strong spin polarization which splits the Fe 3d orbitals, stabilizing the occupied spin-up and destabilizing the unoccupied spin-down orbitals (right side). The terminal C_6H_5 up-spin/down-spin pairs ($8a_2$ ↑/$9a_2$ ↓) are also split, but much less than the d orbitals. At the central phenyls the spin density is zero by symmetry; therefore, we find up-spin/down-spin pairs not

Table 1. Principal Contributions (%) to the Most Important Orbitals (See Figure 3) from the Mulliken Population Analysis for $Fe_2(NCH_2)_2(NCH)_2(C_6H_5)_2$[a]

		Fe(right)					NCH_2*(middle)				C_6H_5(right)			NCH(right)	
	ϵ_i, eV	d_{z^2}	$d_{x^2-y^2}$	d_{xz}	d_{yz}	d_{xy}	$3a_g$	$3b_u$	$3a_u$	$3b_g$	12a′	2a″	3a″	4a′	2a″
unoccupied orbitals															
21a″ ↑	−2.05			2											91
50a′ ↓	−2.79	52						13							
20a″ ↓	−3.05			50	5										16
49a′ ↓	−3.56					51					10				
48a′ ↓	−4.01		66												
occupied orbitals															
19a″ ↓	−4.03				76								10		
47a′ ↑[b]	−4.65	10	5			5		6			30				
18a″ ↑	−4.82			36					7	33					2
46a′ ↑[b]	−5.68	25				23		14			10			5	
17a″ ↑	−5.79				65								23		2
45a′ ↓	−6.20	5	6			17					59				
16a″ ↓	−6.33												91		
15a″ ↓	−6.40											95			
14a″ ↑	−6.42											99			
13a″ ↑	−6.52				23					4			67		
44a′ ↑	−6.82	5	58			10	3	7							
43a′ ↑	−7.22	43						44							
12a″ ↑[b]	−7.24			39					4	38					
42a′ ↑	−7.38	4	17			36					28				
8a″ ↑	−10.68			13					71						
30a′ ↑	−11.66		4				44								

[a] To each spin-up (-down) orbital corresponds a degenerate spin-down (-up) partner, which is its spatial mirror image, in the left side of the molecule. [b] These orbitals also have some amplitude on the left side: 47a′ ↑, 17% $3d_{z^2}$ Fe(left); 46a′ ↑, 7% $3d_{z^2}$ Fe(left); 12a″ ↑, 12% $3d_{xz}$ Fe(left).

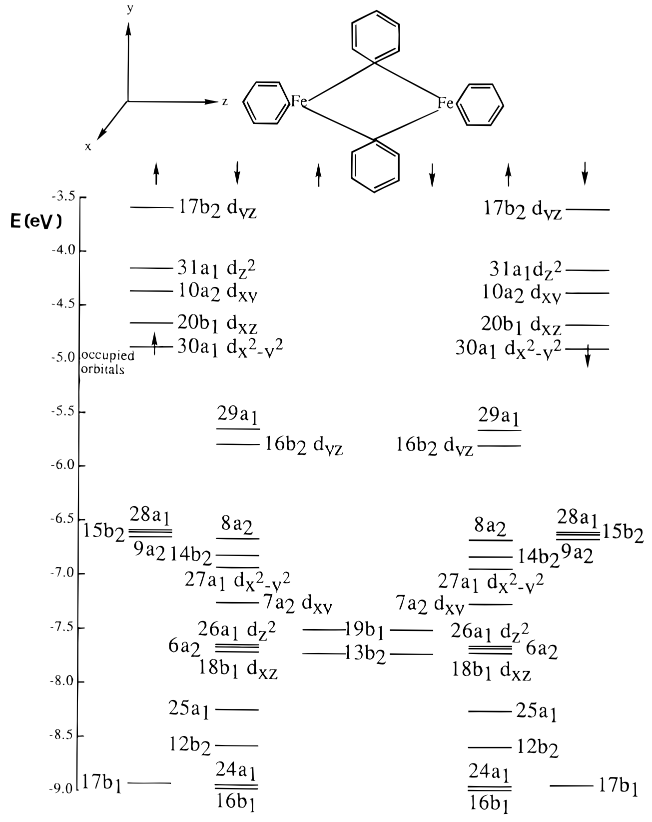

Figure 4. Energy levels for the broken symmetry state of $Fe_2(C_6H_5)_4$. The orbitals are grouped according to their distribution on the left, center, or right of the molecule. Spin-up levels are shown below the up arrows; spin-down, below the down arrows. The six occupied and four unoccupied orbitals with mainly Fe 3d character are explicitly labeled.

split, and one is the degenerate mirror image of the other. The weak overlap between the up-spin and down-spin magnetic orbitals (via the C_6H_5* groups) leads to a very probable antiferromagnetic coupling of superexchange type.

(b) Population Analyses. Table 2 shows the Mulliken population analysis of complex **5** for the most relevant occupied and virtual orbitals in terms of Fe and C_6H_5 fragment components. The most interesting SCF atomic orbitals for the Fe atom and molecular orbitals for the phenyl radical are considered. We can describe the ligand $5b_1$ orbital as a low-lying, doubly occupied MO, containing the combination of the p_x orbitals of the C atoms (for a molecule placed in the *xz* plane). Higher in energy, the $1a_2$ and $2b_2$ doubly occupied orbitals constitute, respectively, in C_{2v} symmetry, the two π combinations of C p_y orbitals. Finally, the highest in energy, singly occupied ligand orbital turns out to be $7a_1$, which is an sp_z hybrid orbital, localized on the C atom not bonded to H. In a calculation performed on the two bridging ligands, occupying the same position as in the overall molecule, we found that, in D_{2h} symmetry, the two $7a_1$ orbitals give rise to a bonding combination, $7a_{1g}$ ($7a_1 + 7a_1$), and to an antibonding one, $7b_{2u}$, ($7a_1 - 7a_1$). Analogously, the two $2b_2$ orbitals interact, originating a $2b_{1u}$ ($2b_2 - 2b_2$) orbital, and a $2b_{3g}$ ($2b_2 + 2b_2$) orbital. The $1a_2$/$1a_2$ combination gives a $1a_{1u}$ ($1a_2 + 1a_2$) orbital and a $1b_{2g}$ ($1a_2 - 1a_2$) orbital, almost degenerate. If we focus on the right side of the molecule, as in the previous case, we see that all occupied α orbitals show a certain Fe 3d character. Analogously to what was observed for complex **4**, most of the orbitals reported in Table 2 are delocalized on the metals and the bridging or terminal ligands. The complete identification of the magnetic orbitals is easier than for complex **4**. We identified them as $18b_1$, $7a_2$, $26a_1$, $27a_1$, and $16b_2$, corresponding mainly to $3d_{xz}$, $3d_{xy}$, $3d_{z^2}$, $3d_{x^2-y^2}$, and $3d_{yz}$, respectively. The Fe $3d_{x^2-y^2}$ orbital turns out to be the doubly occupied one in this complex. We performed also two more different broken-symmetry, spin-unrestricted calculations, doubly occupying the Fe $3d_{xy}$ orbital, and the Fe $3d_{xz}$, because these two orbitals are the most weakly interacting orbitals together with $3d_{x^2-y^2}$. The two resulting broken symmetry states localized at higher energy (−25.69 eV for the state with doubly occupied $3d_{xy}$ and −25.46 eV for the state with doubly occupied $3d_{xz}$ against the −26.01 eV for the state with doubly occupied $3d_{x^2-y^2}$). These data, together with the energy level diagram, are again consistent with Fe^{2+} d^6 sites. According to our analysis, a very relevant antiferromagnetic

Table 2. Principal Contributions (%) to the Most Important Orbitals (See Figure 4) from the Mulliken Population Analysis for $Fe_2(C_6H_5)_4$[a]

		Fe(right)					C_6H_5*(middle)						C_6H_5(right)			
	ϵ_i, eV	d_{z^2}	$d_{x^2-y^2}$	d_{xz}	d_{yz}	d_{xy}	$7a_{1g}$	$1b_{2g}$	$2b_{3g}$	$1a_{1u}$	$2b_{1u}$	$7b_{2u}$	$7a_1$	$1a_2$	$2b_2$	$5b_1$
unoccupied orbitals																
$17b_2\downarrow$	−3.59				49							20				
$31a_1\downarrow$	−4.16	46									8		12			
$10a_2\downarrow$	−4.37					95										
$20b_1\downarrow$	−4.67			94												
occupied orbitals																
$30a_1\downarrow$	−4.89	4	82													
$29a_1\uparrow$	−5.64	14											45			
$16b_2\uparrow^b$	−5.79				28							15			23	
$28a_1\downarrow$	−6.59	20											44			
$15b_2\downarrow^b$	−6.61														69	
$9a_2\downarrow$	−6.65													100		
$8a_2\uparrow$	−6.67													99		
$14b_2\uparrow^b$	−6.82											9			49	
$27a_1\uparrow$	−6.93		67								8					
$7a_2\uparrow$	−7.26					53				43						
$19b_1\updownarrow$	−7.5							99								
$26a_1\uparrow$	−7.64	30					18				17		16			
$6a_2\uparrow$	−7.67					42				56						
$18b_1\uparrow$	−7.71			90												3
$13b_2\updownarrow^b$	−7.73								87							
$25a_1\uparrow$	−8.25	12	14								56					
$12b_2\uparrow$	−8.58				47							29				
$17b_1\downarrow$	−8.93															99
$24a_1\uparrow$	−8.95	23					32									
$16b_1\uparrow$	−8.98			3												97

[a] To each spin-up (-down) orbital corresponds a degenerate spin-down (-up) partner, which is its spatial mirror image, in the left side of the molecule. The double arrow $\updownarrow$ indicates degenerate α/β orbitals referring to the central phenyls. [b] These orbitals also have some amplitude on the left side: $16b_2\uparrow$, 16% $3d_{yz}$ Fe(left), 6% $2b_2$ C_6H_5(left); $15b_2\downarrow$, 26% $2b_2$ C_6H_5(left); $14b_2\uparrow$, 11% $3d_{yz}$ Fe(left), 21% $2b_2$ C_6H_5(left); $13b_2\updownarrow$, 5% $3d_{yz}$ Fe(left).

coupling is more reasonably expected in $Fe_2(C_6H_5)_4$ rather than a direct iron−iron bond (see later discussion).

Heisenberg Coupling Constants. In order to analyze spin coupling, the energy E_B of the broken symmetry state Ψ_B must be related, through the Heisenberg exchange coupling constant J, to the energy $E(S_{max})$ of the high-spin state $\Psi(S_{max})$, as we pointed out in the first section.[16] The broken symmetry state for the two systems is described by the energy level structure in Figures 3 and 4 we have already commented on, and we can refer to it as the low-spin and antiferromagnetic (AF) configuration. The high-spin states (or ferromagnetic (F) configurations) are constructed in such a way that the spin vectors for the monomer subunits are parallel aligned to give a total $S = S_{max} = 4$ with 8 spin α magnetic electrons and 0 spin β. The ferromagnetic, high-spin states for model complexes **4** and **5** could be obtained as results of independent SCF unrestricted calculations for $S = 4$, in the same symmetry of the corresponding nuclear frameworks (*i.e.*, C_{2h} for complex **4** and D_{2h} for complex **5**).

The same kinds of unrestricted, full symmetry calculations were performed for the alternative double d occupations in both complexes. The differences between the possible situations should give us a feeling about the accuracy we can achieve in the calculation of the Heisenberg coupling constant for these complexes and about the difficulty one can meet with the interpretation of the experimental data. The Heisenberg exchange coupling constant for the two systems can be evaluated using eq 1, and Heisenberg spin ladders can be constructed, constituted by $S_{max} + 1$ different pure spin states having relative energies $E(S) - E(S{-}1) = -2JS$ for $0 \le S \le S_{max}$. The schematic and general diagram is shown in Figure 5. We note that the singlet−triplet splitting is $2J$ and that the energy difference between $\Psi(S_{max})$ and the singlet (ground) state is

$$E(S_{max}) - E(S{=}0) = -S_{max}(S_{max} + 1)J$$

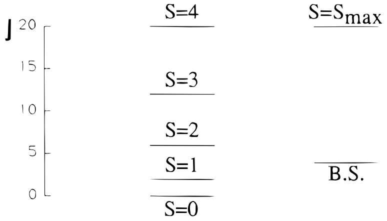

Figure 5. General diagram for the Heisenberg spin ladder of a system with two coupled metallic sites (BS = broken symmetry).

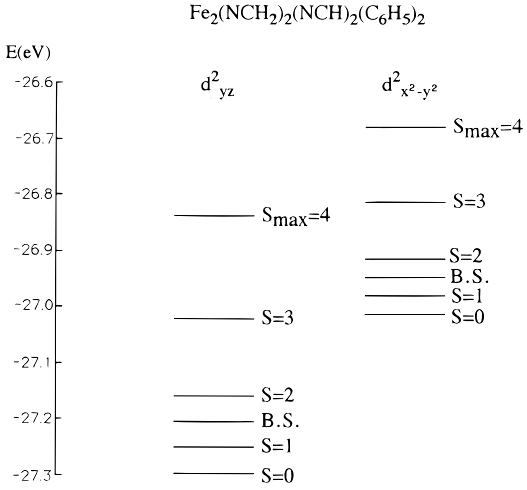

Figure 6. Schematic diagram for the Heisenberg spin ladders of $Fe_2(NCH_2)_2(NCH)_2(C_6H_5)_2$ calculated for alternative double d occupations (BS = broken symmetry).

The singlet has energy $5|J|$ below the broken symmetry energy. In Figures 6 and 7 the alternative computed Heisenberg spin ladders are shown for model complexes **4** and **5**, respectively. The theoretical values we calculated are $J = -185$ cm^{-1} for $Fe_2(NCH_2)_2(NCH)_2(C_6H_5)_2$ with $3d_{yz}$ doubly occupied, $J = -134$ cm^{-1} with $3d_{x^2-y^2}$ doubly occupied, $J = -308$ cm^{-1} for

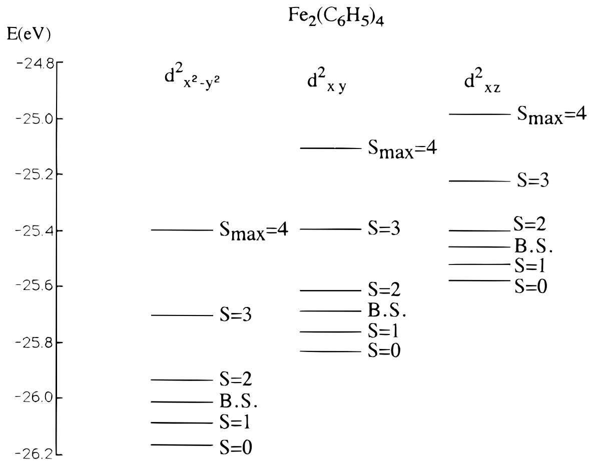

Figure 7. Schematic diagram for the Heisenberg spin ladders of $Fe_2(C_6H_5)_4$ calculated for three different double d occupations (BS = broken symmetry).

$Fe_2(C_6H_5)_4$ with $3d_{x^2-y^2}$ doubly occupied, $J = -293$ cm^{-1} with $3d_{xy}$ doubly occupied, and $J = -239$ cm^{-1} with $3d_{xz}$ doubly occupied. Experimentally, $J = -63.7$ cm^{-1} for complex **1** and $J = -31.5$ cm^{-1} for complex **2**, although the latter data refer to the average coupling of only three out of the four unpaired electrons on each Fe(II) center (see ref 2). However, discrepancies of this size between theory and experiment are not unexpected, because of the very small relevant energy differences involved in these calculations.[17] Although previous broken symmetry calculations[12] gave rather satisfactory results, the considered compounds were dinuclear species with simple bridging ligands, like S^{2-} ions. On the other hand, in the considered complexes **4** and **5** the bridging ligands are rather complex molecules so that the results of the broken symmetry calculations could be less accurate and also more sensitive to changes in the nature of the ligand, like those introduced in the simplified models. Indeed, it must be recalled that the considered model molecules **4** and **5** are different from the actual complexes **1** and **2**. In particular, the substitution of a mesityl ring with a hydrogen or a phenyl group could lead to relevant changing in the ordering and nature of the frontier orbitals for the bridging ligands, and this is known to affect the values of the superexchange coupling constants.[18]

For complex **2**, for which the discrepancy is higher, we also have to take into account that the magnetic susceptibility data have been fitted by using a generalized Hamiltonian form instead of the simple Heisenberg spin Hamiltonian.[2] The Heisenberg model seemed not to be completely appropriate for the description of the system, and this could explain the higher discrepancy between the calculated and experimentally deduced values of the coupling constants.

Metal−Metal Bonding. From our study on compounds **4** and **5** it is clear that we must exclude the presence of a direct iron−iron bond. Looking at the energy level diagrams for the broken-symmetry states of the two compounds, we are not able to identify any MO's that are metallic in character and bonding, containing a comparable percentage of a certain d orbital of Fe right and Fe left. This is the condition which must be fulfilled in order to speak of a bond between two symmetric and degenerate fragments. The short Fe−Fe distance found especially in complex **5** should be ascribed essentially to strong iron bridging ligand interactions. This is not too strange, since it has been established already that the short bond distance is not a good criterion for unequivocally proving the presence of the bond.[3]

Table 3. Binding Energies for the Lowest States of Different Spin Symmetry (Broken Symmetry Singlet, Triplet, Quintet, Septet, and Nonet) of the $Fe_2(HNCH)_4$ Complex

occupation[a]	symmetry	S	$E(S)$ (eV)
$20a\uparrow20b\uparrow18a\downarrow18b\downarrow$	C_2	2	−26.508
$38a\uparrow38a\downarrow$	broken symmetry C_1	0	−26.147
$20a\uparrow19b\uparrow19a\downarrow18b\downarrow$	C_2	1	−25.977
$21a\uparrow20b\uparrow18a\downarrow17b\downarrow$	C_2	3	−25.001
$21a\uparrow21b\uparrow17a\downarrow17b\downarrow$	C_2	4	−23.152

[a] The highest occupied orbitals for each symmetry and spin index are reported.

$Fe_2(HNCH)_4$ Complex. (a) Energy Level Structure. A list of the binding energies for the lowest spin states of complex **6**, on which unrestricted calculations have been performed, is reported in Table 3. From these data, we see that the ground state is the quintet ^{5}A with the first excited state, a ^{3}B, 0.53 eV above in energy. Actually, in spite of many attempts, it has been not possible to converge to a singlet state wave function: the lowest singlet is probably a high-energy excited state. Anyway, the interpretation of the magnetization data (see below) shows inequivocably that compound **3** has an isolated $S = 2$ ground state so that we can confidently assume that ^{5}A is the true ground state for complex **6**.

In a MO picture a low-lying $S = 2$ state implies four quasi-degenerate singly occupied molecular orbitals. Correspondingly, the reason for the failure to converge the unrestricted procedure in the singlet state could be due to a bad representation of the quasi-degeneracy correlation. Although such effects could make questionable the purely theoretical assignment of the $S = 2$ ground state, this conclusion is assured by the magnetic data.

(b) Magnetism. The high excitation energies found for all of the excited states prevents their thermal population, so that the forecast magnetic behavior is that of an isolated quintet state and then follows the Curie law; *i.e*, a horizontal straight line is observed for μ_{eff} vs T, with μ_{eff} (per iron) $= g\sqrt{3}$. Eventually, a fall of μ_{eff} at low temperatures could be observed because of zero field splitting, which is commonly found for Fe(II) species.[19] This forecast behavior is qualitatively compatible with the observed magnetic data for μ_{eff} vs T, provided that anomalously high values for both g and D are assumed.

Moreover, these considerations suggest that the observed magnetic data should be interpreted by using a phenomenological model, different from that used by Floriani and co-workers in ref 2, in which each dimer is considered an isolated spin center with $S = 2$.

We have therefore performed a new quantitative fit of the magnetic data for complex **3**, using the axial spin Hamiltonian

$$\hat{H} = \beta g_{\parallel} H_z \hat{S}_z + \beta g_{\perp}(H_x\hat{S}_x + H_y\hat{S}_y) + D[\hat{S}_z^{\,2} - S(S+1)/3] \quad (2)$$

where D is the axial zero field splitting constant, which leads to the following temperature dependence of the parallel and perpendicular magnetic susceptibilities[19,20]

$$\chi_{\parallel} = \frac{Ng_{\parallel}^{\,2}\beta^2}{kT}\,\frac{2\exp(-D/kT) + 8\exp(-4D/kT)}{1 + 2\exp(-D/kT) + 2\exp(-4D/kT)} \quad (3)$$

$$\begin{aligned}\chi_{\perp} = {} & [Ng_{\perp}^{\,2}\beta^2/kT][(6kT/D)(1 - \exp(-D/kT)) + \\ & (4kT/3D)(\exp(-D/kT) - \exp(-4D/kT))]/[1 + \\ & 2\exp(-D/kT) + 2\exp(-4D/kT)]\end{aligned} \quad (4)$$

The average magnetic susceptibility for a powdered sample is then given by $\chi = (\chi_{\parallel} + 2\chi_{\perp})/3$.

---

(17) De Loth, P.; Cassoux, P.; Daudey, J. P.; Malrieu, J. P. *J. Am. Chem. Soc.* **1981**, *103*, 4007.

(18) Willet, R. D.; Gatteschi, D.; Kahn, O. In *Magneto-Structural Correlations in Exchange Coupled Systems*; NATO ASI Series; Reidel: Dordrecht, The Netherlands, 1985.

(19) Carlin, R. L. *Magnetochemistry*; Springer-Verlag: Berlin, Germany, 1986.

(20) Kahn, O. *Molecular Magnetism*; VCH: New York, 1993.

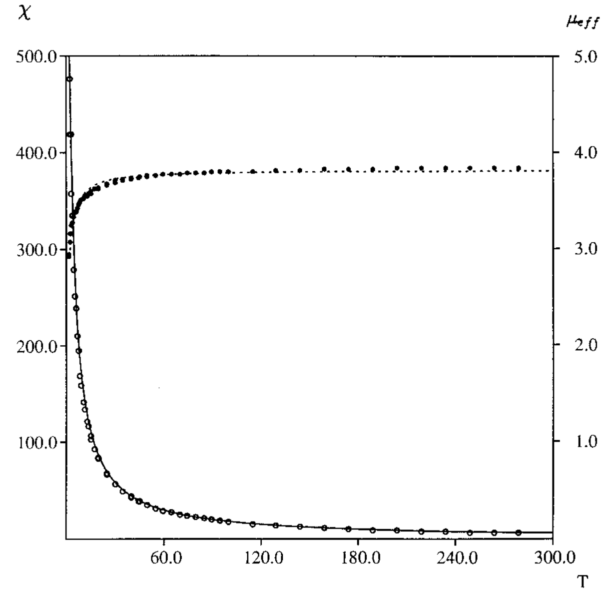

Figure 8. Magnetic susceptibility (empty circles) (10^{-3} cm^3 mol^{-1}) and effective magnetic moment (filled circles) (μ_B) per dimer of **3** as a function of the temperature. The solid and dashed lines are the best theoretical fits (see text) to the experimental data.

A good fit to the collected data for complex **3** yielded $g_{\|} = 2.65$, $g_{\perp} = 1.95$, $D = 2.9$ cm^{-1} and is shown in Figure 8. The average g value corresponding to the anisotropic values obtained in this fitting is $g = (g_{\|} + 2g_{\perp})/3 = 2.18$. Although the differences between $g_{\|}$ and $g_{\perp}$ are usually neglected in the fitting of data for powdered samples taking a unique average g value, the strong axial anisotropy in molecule **3** prevents one from using this simplification; indeed, the use of an average g parameter leads to a much poorer fitting. Note that both g and D values are fairly high but still in the range for iron(II) compounds.[19,21] These high values of g and D can be related with the results of the MO calculations. Indeed, these calculations have shown the presence of low-lying excited states, namely, the triplet and maybe the singlet, high enough in energy to be totally depopulated at room temperature. Therefore, there should be a relevant coupling between the ground $S = 2$ and these excited states through the spin−orbit coupling which is expected to produce both a large deviation of g from its spin-only value and a relevant zero field splitting.

The theoretical results discussed above have then led to an interpretation of the experimental magnetic data which is different from the original interpretation of ref 2, although in perfectly equivalent agreement: the observed behavior for μ_{eff} vs T cannot distinguish between the two interpretations.

However, it would be possible to distinguish between these two interpretations by studying the magnetization of compound **3** at high fields. Indeed, if the system is described as two slightly interacting spin centers with $S = {}^3/_2$ and $g = 1.98$, as done in ref 2, we would forecast a saturation of M/Nμ_B to $2gS$ per dimer, *i.e.*, to about 6, while if the system is described by one spin center with $S = 2$ and $g = 2.18$, as done here, we would forecast a saturation of M/Nμ_B to gS per dimer, *i.e.*, to about 4.4, or, better, lower because of the relevant zero field splitting, which is known to reduce the magnetization values with respect to the Brillouin curve.[22]

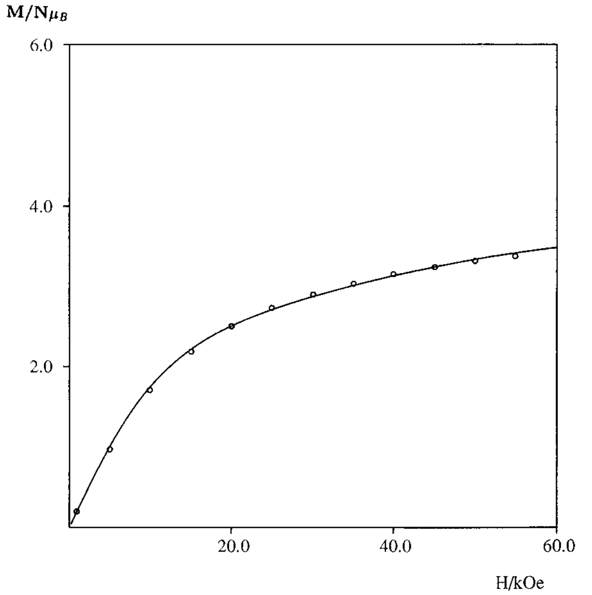

Figure 9. Magnetization, as M/Nμ_B, per dimer of **3** as a function of the field at 1.9 K. The solid line is the best theoretical fit (see text) to the experimental data.

To choose between the two interpretations, isothermal variable-field magnetization measurements were taken at 1.9 K, up to 5.5 T, and the data are shown in Figure 9. We see that at the highest measuring field of 5.5 T the magnetization is close to saturation with a value of M/Nμ_B of about 3.4: this suggests that the model of the dimer as one spin center with $S = 2$ proposed in this paper is more appropriate. However, to confirm this conclusion, it would be desirable to perform a quantitative fitting of the magnetization data vs the field H with the same model used for the fitting of μ_{eff} vs T and check the consistency of the results.

First of all, we recall that for a molecule such as complex **3** which has an isolated spin multiplet as ground state, the variation of the magnetization with H/T is described by the Brillouin function, *i.e.*, by the expression

$$M = Ng\mu_B SB_2(z) \qquad (5)$$

where $z = g\mu_B H/kT$ and $B_2(z)$ is the Brillouin function for $S = 2$ state.[19] From Figure 9 we see that M/Nμ_B saturates at a value of about 3.4, which is much less than 4.4, forecast by eq 5 for $g = 2.18$. It must, however, be considered that, due to the relevant zero field splitting, the $S = 2$ ground state is split into three $M_S = 0, \pm1, \pm2$ components, and the magnetization does not follow the Brillouin behavior anymore.[22] The correct dependence of the magnetization as a function of the field H can be obtained through the full-matrix diagonalization of the Hamiltonian matrix, using the five spin functions of the $S = 2$ state and the Hamiltonian of eq 2. The obtained eigenvalues E_i and their derivatives with respect to the magnetic field were used to calculate the magnetization with the following basic thermodynamic relation:[20]

$$M = \frac{N\sum_i(-\partial E_i/\partial H)\exp(-E_i/kT)}{\sum_i \exp(-E_i/kT)} \qquad (6)$$

In the presence of a zero field splitting the magnetization becomes anisotropic, but an average magnetization for a

---

(21) Casey, A. T.; Mitra, S. In *Theory and Applications of Molecular Paramagnetism*; Bodreaux, E. A., Mulay, L. N., Eds.; Wiley: New York, 1976; p 135.

(22) Vincent, J. B.; Christmas, C.; Chang, H. R.; Li, Q.; Boyd, P. D. W.; Huffman, J. C.; Hendrickson, D. N.; Cristou, G. *J. Am. Chem. Soc.* **1989**, *111*, 2086.

(23) Davy, R. D.; Hall, M. B. *J. Am. Chem. Soc.* **1989**, *111*, 1268.

(24) Poumbga, C.; Daniel, C.; Benard, M.; Huffman, J. C.; Hendrickson, D. N.; Cristou, G. *J. Am. Chem. Soc.*, **1991**, *113*, 1090.

polycrystalline sample can be obtained as $M = (M_{\parallel} + 2M_{\perp})/3$. The best fit of the magnetization data in Figure 9 was obtained for $g_{\parallel} = 2.40$, $g_{\perp} = 1.95$, and $D = 2.7$ cm^{-1} and is shown as a solid line in Figure 9. Note that these values agree very well with those obtained from the variable-temperature magnetic susceptibility fitting, the small observed differences being easily explained in terms of the neglected effects of rhombic distorsion, monomeric impurities, and intermolecular interactions. This agreement between the parameters obtained in the two fittings, μ_{eff} vs T and M vs H, confirms both the goodness of our phenomenological model and the nature of the spin quintet for the ground state of compound **3**.

(c) Bonding. An intuitive description of bonding in compound **6** according to the ionic and covalent models which are commonly used in organometallic chemistry implies first the donation of the 4s valence electrons from iron to two of the HNCH ligands. This would lead to a charged system with two Fe^{2+} and four $HNCH^-$ subunits. Each iron ion, with a d^6 configuration, accepts one electron pair from each ligand (two from carbon and two from nitrogen) forming two Fe−N and two Fe−C bonds, and then there is a further interaction of the Fe 3d orbitals with the π ligands system and the 3d orbitals of the other iron. Due to the low symmetry, C_2, of this compound, it is difficult to extract all of these features from the wave function, so we will limit it to metal−metal and metal−π-ligands system interactions.

We will discuss here only the ground state ^{5}A wave function. The results of our unrestricted calculations on this state are presented in Table 4, in which we report the Mulliken population analysis of the most relevant molecular orbitals in terms of metal and ligand orbitals. We will focus here on those orbitals with major metal character which are primarily responsible for metal−metal bonding.

A first examination of Table 4 shows that (i) there is a relevant spin-polarization effect, the orbitals which are simultaneously spin-up and spin-down being fairly different both in energy and in the relative metal and ligand contributions, (ii) the four unpaired orbitals are of mainly metal character, although two of them, 20b and 20a, show a relevant ligand character (the 19b is an almost pure π^*, while the other three show almost equivalently mixed σ and δ bonding character), and (iii) almost all of the upper valence bioccupied orbitals have a strongly mixed metal and ligand character. The ligand orbitals more involved in these MO are 5a′ and 2a″. Orbital 5a′ contains the unpaired electron of the HNCH radical and corresponds to a combination of the carbon and nitrogen lone pairs. Orbital 2a″ is unoccupied and corresponds to the C−N π^* orbital. The combination of the two bridging HNCH ligands taken together in the C_2 symmetry gives rise to two combinations of the 5a′ orbitals of a (5a′ + 5a′) and b (5a′ − 5a′) symmetry and two combinations of the 2a″ orbitals of a (2a″ + 2a″) and b (2a″ − 2a″) symmetry. Contour plots are presented in Figure 10 for a few molecular orbitals which are more significant for metal−metal bonding. From Figure 10 we can clearly see the Fe−Fe π character of the 17a orbital, the π^* character of the 19b orbital, the mixed σ and δ bonding character of the 16a orbital, and the mixed σ and δ antibonding character of the 20b orbital, all of spin-up type, the spin-down corresponding orbitals being qualitatively similar.

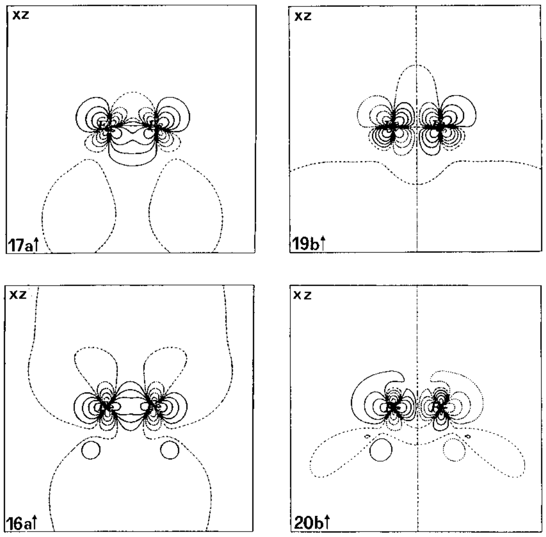

Figure 10. Contour maps for the occupied orbitals 17a ↑ (plotted in *xz* plane), 19b ↑ (plotted in *xz* plane), 16a ↑ (plotted in *xz* plane), and 20b ↑ (plotted in *xz* plane) of $Fe_2(HNCH)_4$. Contour values are 0, ±0.001, ±0.002, ±0.005, ±0.01, ±0.02, ±0.05, ±0.1, ±0.2, and ±0.5 (e/bohr^3)$^{1/2}$.

Table 4. Principal Contributions (%) to the Most Important Orbitals from the Mulliken Population Analysis for $Fe_2(HNCH)_4$

		Fe					HNCH*		HNCH	
	ϵ_i, eV	d_{z^2}	$d_{x^2-y^2}$	d_{xz}	d_{yz}	d_{xy}	5a′	2a″	5a′	2a″
(a) Spin-Up Orbitals										
unoccupied orbitals										
23a ↑	−0.91				19		22	28	14	
23b ↑	−1.03						10	46	15	
22b ↑	−1.30				18			37	20	
22a ↑	−1.37							59	10	14
21b ↑	−1.89									89
21a ↑	−2.02									78
occupied orbitals										
20b ↑	−3.74	12	40				11			7
20a ↑	−4.04	25				20	18		17	
19b ↑	−4.40			82						
19a ↑	−4.63	31	20			17				
18b ↑	−4.94	48	13		9	10				
18a ↑	−4.95		14	25		31	6		8	
17b ↑	−5.25	16			16	34	15			
17a ↑	−5.74		21	56			6		4	
16a ↑	−6.26	25	34				10		15	
16b ↑	−6.29				15		10		38	
15b ↑	−6.64		15			34	31		8	
15a ↑	−7.11				44	12	17		18	
(b) Spin-Down Orbitals										
unoccupied orbitals										
23a ↓	−0.17				34		18		17	
23b ↓	−0.28		12		22	14	11		25	
22b ↓	−0.70	9	11		12			58		
22a ↓	−1.31							83		
21b ↓	−1.47	16	13							49
21a ↓	−1.69					25				65
20b ↓	−2.42	17	21	10						35
19b ↓	−2.60			73						
20a ↓	−2.68	55	7			11				
19a ↓	−2.97	17			15	38				18
occupied orbitals										
18b ↓	−3.44	29	15		11	27				
18a ↓	−3.61		24	54						
17b ↓	−3.99	20			13	25		24		
17a ↓	−4.36		48	27						
16a ↓	−5.55	11					33		31	
16b ↓	−5.95				10		20		50	
15b ↓	−6.07		10			18	44		13	
15a ↓	−6.44				36	10	20		29	

When we consider the overall description of the Fe−Fe bond which comes out from our results, trying to estimate the bond order and its formulation in terms of σ, π, and δ occupancies, many difficulties are encountered. First of all isolation of the Fe_2 as a hypotethical entity within the complex is conceptually difficult: the HNCH ligands strongly distort the metal-centered orbitals, and the through-bond effects via the bridging ligands strongly compete with the through-space direct Fe−Fe interactions. The partition of the Fe−Fe interaction into σ, π, and δ

Table 5. Symmetry Properties of the Fe d Bonding and Antibonding Combinations in the C_2 Group

symmetry	A	B
combination	$\sigma(d_{z^2})$ $\pi(d_{xz})$ $\pi^*(d_{yz})$ $\delta(d_{x^2-y^2})$ $\delta^*(d_{xy})$	$\sigma^*(d_{z^2})$ $\pi^*(d_{xz})$ $\pi(d_{yz})$ $\delta^*(d_{x^2-y^2})$ $\delta(d_{xy})$

Table 6. Bonding and Antibonding Populations and Bond Orders for the Various Components of the Fe−Fe d Orbitals

component	$\sigma(d_{z^2})$	$\pi(d_{xz})$	$\pi(d_{yz})$	$\delta(d_{x^2-y^2})$	$\delta(d_{xy})$
bonding populations	0.92	1.62	0.74	1.61	1.48
antibonding populations	1.25	0.82	0.95	0.93	0.90
net bond order	−0.16	0.40	−0.10	0.34	0.29

components is therefore fairly arbitrary. Moreover, the analysis in terms of these components of metal−metal bond is complicated by the low symmetry of the molecule. Indeed, under C_2, the A representation contains the bonding combinations of $\sigma(d_{z^2})$, $\pi(d_{xz})$, and $\delta(d_{x^2-y^2})$ and the antibonding combinations of $\pi^*(d_{yz})$ and $\delta^*(d_{xy})$ of the two irons, while the B representation contains the corresponding opposite combinations. The σ, π, and δ components of metal−metal bond are then completely mixed in both representations, so that a definite character cannot be attributed to the upper valence molecular orbitals. The symmetry properties of the Fe 3d orbitals with respect to the Fe−Fe bonding in the C_2 group are reported in Table 5.

Formal bond orders for each of the three components can be calculated from the unrestricted wave function as

$$\mathrm{BO}(\Gamma) = {}^1/_2\Big[\sum_i^{\mathrm{MO}} \rho^i_{\mathrm{Fe}_2}(\Gamma) - \rho^i_{\mathrm{Fe}_2}(\Gamma^*)\Big] \qquad (7)$$

in which $\rho^i_{\mathrm{Fe}_2}(\Gamma)$ or $\rho^i_{\mathrm{Fe}_2}(\Gamma^*)$ is the amount of the population of orbital i which can be attributed to the bonding or antibonding component Γ ($\Gamma = \sigma, \pi, \delta$) of the dimetal unit according to the Mulliken population analysis. For our unrestricted calculation the summation on i is extended over all of the occupied spin-up and spin-down orbitals, and corresponds to an average of these components. The computed values, including the separate Γ and Γ^* contributions, are reported in Table 6. We can see that the metal−metal interaction can be qualitatively described in terms of a π and a δ bond of order of approximatively half, without any net σ bond contribution.

These results show that the short Fe−Fe length does not seem to be due to strong direct metal−metal interactions but rather to metal−ligand interactions and suggests that the short Fe−Fe distance is in large part the result of the bridging ligands holding the iron atoms in place.

From Table 4 we can also see that most of the molecular orbitals which contribute to Fe−Fe bonding also present a relevant ligand character, so that it is not possible to unravel completely the metal−metal bonding from the metal−ligand one.

The Fe−Fe bonding shows therefore a complex nature which can be rationalized, noting that the 3d occupations are determined as a compromise between the metal−metal and the metal−ligand interactions. Indeed, it is possible to lower the energy of the complex occupying a Fe−Fe antibonding orbital instead of a Fe−Fe bonding orbital if the former has a strong metal−ligand character. This effect is well-known, for istance, for edge sharing dinuclear octahedral complexes.[3] In our case all of the five Fe−Fe 3d antibonding combinations are suitably oriented to be stabilized through the interaction with the lowlying unoccupied 2a″ ligand orbital, of C−N π^* character (see Figure 11).

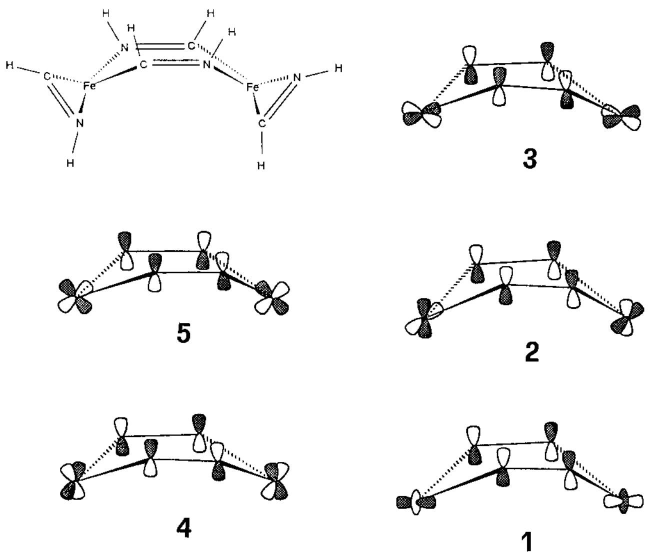

Figure 11. Schematic representations of the orbital interactions between the two a and b combinations of the bridging ligand orbitals 2a″ and the metal−metal antibonding orbital combinations: (1) (2a″ − 2a″) − $\sigma(d_{z^2})$, b symmetry; (2) (2a″ − 2a″) − $\delta(d_{x^2-y^2})$, b symmetry; (3) (2a″ + 2a″) − $\pi^*(d_{yz})$, a symmetry; (4) (2a″ + 2a″) − $\delta(d_{xy})$, a symmetry; (5) (2a″ − 2a″) − $\pi^*(d_{xz})$, b symmetry.

Indeed, the $\delta^*(xy)$ and $\pi^*(yz)$ orbitals interact with the ligand orbital combination 2a″ + 2a″ of a symmetry, while the σ^*, $\delta^*(x^2-y^2)$ and $\pi^*(xz)$ orbitals interact with the ligand orbital combination 2a″ − 2a″ of b symmetry.

Strongly mixed with the MO's of more relevant metal character is also the highest occupied 5a′ ligand orbital, which describes the C and N lone pairs responsible of the Fe−N and Fe−C bonding. However, due to the entangled nature of this mixing, it has not been possible to unravel the metal−metal combinations implied in these interactions.

Short metal−metal distances due to metal−ligand interactions rather than to metal−metal ones have been reported for multiple Cr−Cr and V−V bonds.[23,24]

4. Conclusions

The results obtained for model compounds **4** and **5** have clearly established that (i) there is no direct Fe−Fe bond, (ii) the reduction of the magnetic moment is due only to antiferromagnetic interactions via bridging ligands, and (iii) the fairly short metal−metal distance in compound **2** is due to strong metal−bridging ligands interactions. Heisenberg coupling constants were also evaluated for these two complexes, showing a strong antiferromagnetic coupling between the two iron centers, although the agreement between calculated and observed data is not completely satisfactory.

Calculations on complex **6** have shown that the ground state is an isolated spin quintet, a result which has been confirmed by the experimental magnetization data. Moreover, our calculations have shown that the direct Fe−Fe interaction is not especially strong and can only partially represent the driving force toward the very short metal−metal distance, suggesting that the relative positions of the metal atoms could be strongly conditioned by their interactions with bridging ligands.

Acknowledgment. The present work has been carried out within the COST D3 Action. We thank the CINECA for providing a computer grant and P.B. thanks the ESF REHE Programme for providing a scholarship.

IC9507676